Revision of the Single-Channel Algorithm for Land Surface Temperature Retrieval From Landsat Thermal-Infrared Data

Juan C. Jiménez-Muñoz, Jordi Cristóbal, José A. Sobrino, Guillem Sòria, Miquel Ninyerola, and Xavier Pons

***Abstract*—This paper presents a revision, an update, and an extension of the generalized single-channel (SC) algorithm developed by Jiménez-Muñoz and Sobrino (2003), which was particularized to the thermal-infrared (TIR) channel (band 6) located in the Landsat-5 Thematic Mapper (TM) sensor. The SC algorithm relies on the concept of atmospheric functions (AFs) which are dependent on atmospheric transmissivity and upwelling and downwelling atmospheric radiances. These AFs are fitted versus the atmospheric water vapor content for operational purposes. In this paper, we present updated fits using MODTRAN 4 radiative transfer code, and we also extend the application of the SC algorithm to the TIR channel of the TM sensor onboard the Landsat-4 platform and the enhanced TM plus sensor onboard the Landsat-7 platform. Five different atmospheric sounding databases have been considered to create simulated data used for retrieving AFs and to test the algorithm. The test from independent simulated data provided root mean square error (rmse) values below 1 K in most cases when atmospheric water vapor content is lower than 2 $\mathbf{g \cdot cm^{-2}}$. For values higher than 3 $\mathbf{g \cdot cm^{-2}}$, errors are not acceptable, as what occurs with other SC algorithms. Results were also tested using a land surface temperature map obtained from one Landsat-5 image acquired over an agricultural area using inversion of the radiative transfer equation and the atmospheric profile measured *in situ* at the sensor overpass time. The comparison with this "ground-truth" map provided an rmse of 1.5 K.**

***Index Terms*—Landsat, land surface temperature (LST), single-channel (SC), thermal-infrared (TIR).**

I. Introduction

THERMAL remote sensing is recognized to be a major source of quantitative and qualitative information on land surface processes and for their characterization, analysis, and modeling [1], [2]. The launch of the Landsat series has allowed the acquisition of a historical database (from 1982 to present) of thermal imagery at medium spatial resolution suitable for different environmental studies, for example, evapotranspiration and energy balance component estimations or water resource studies. Thermal-infrared (TIR) data have been collected through band 6 (B6) of the Thematic Mapper (TM) instrument onboard Landsat-4 (L4B6) and Landsat-5 (L5B6) platforms and the enhanced TM plus instrument onboard the Landsat-7 (L7B6) platform.

Land surface temperature (LST) is the key variable to be retrieved from the TIR data. The interest on Landsat TIR data has increased in the last years, which has encouraged the emergence of different publications related to this issue. The most appropriate procedure to retrieve LST from a single-channel (SC) located in the TIR region, as is the case of Landsat series, is by inversion of the radiative transfer equation (RTE) according to the following expression applied to a certain sensor channel (or wavelength interval):

$$B(T_{\rm s}) = \frac{L_{\rm sen} - L^{\uparrow} - \tau(1-\varepsilon)L^{\downarrow}}{\tau\varepsilon} \tag{1}$$

where

B Planck's law, expressed as

$$B_{\lambda}(T) = \frac{c_1}{\lambda^5 \exp\left(\frac{c_2}{\lambda T}\right) - 1} \tag{2}$$

with c_1 and c_2 being the Planck's radiation constants, with values of $1.19104 \cdot 10^8$ $\mathrm{W \cdot \mu m^4 \cdot m^{-2} \cdot sr^{-1}}$ and 14387.7 $\mu\mathrm{m \cdot K}$, respectively;

λ wavelength;

$T_{\rm s}$ land surface temperature (LST);

$L_{\rm sen}$ at-sensor registered radiance;

$L^{\uparrow}$ upwelling atmospheric radiance (path radiance);

τ atmospheric transmissivity;

ε surface emissivity;

$L^{\downarrow}$ downwelling atmospheric radiance.

Radiances are in watts per square meter per steradian per micrometer, and wavelength is in micrometers.

Examples of this procedure can be found in [3] and [4]. The main problem when using (1) is that atmospheric parameters τ, $L^{\uparrow}$, and $L^{\downarrow}$ must to be known. This implies the availability of atmospheric soundings launched near the study area and near the acquisition time of the satellite image. Currently, this problem is

Manuscript received January 28, 2008; revised July 21, 2008 and September 3, 2008. First published November 25, 2008; current version published December 17, 2008. This work was supported in part by the European Space Agency (SEN2FLEX, project RFQ 3-11291/05/I-EC) and in part by Ministerio de Ciencia y Tecnología (TERMASAT, project ESP2005-07724-C05-04).

J. C. Jiménez-Muñoz, J. A. Sobrino, and G. Sòria are with the Global Change Unit, Department of Earth Physics and Thermodynamics, University of Valencia, 46100 Valencia, Spain (e-mail: jcjm@uv.es; jose.a.sobrino@uv.es).

J. Cristóbal is with the Department of Geography, Autonomous University of Barcelona, 08193 Cerdanyola del Vallès, Spain (e-mail: jordi.cristobal@uab.es).

M. Ninyerola is with the Unit of Botany, Department of Animal Biology, Plant Biology and Ecology, Autonomous University of Barcelona, 08193 Cerdanyola del Vallès, Spain (e-mail: miquel.ninyerola@uab.es).

X. Pons is with the Department of Geography, Autonomous University of Barcelona, 08193 Cerdanyola del Vallès, Spain, and also with the Centre for Ecological Research and Forestry Applications, 08193 Cerdanyola del Vallès, Spain (e-mail: xavier.pons@uab.es).

solved by using National Centers for Environmental Prediction (NCEP) modeled atmospheric profiles, but these data are useful only on a global scale, and they need to be interpolated to a particular date, time, and location. A web-based tool for atmospheric correction of Landsat-5 and Landsat-7 TIR data from NCEP was proposed by Barsi *et al.* [5], [6].

In order to avoid the dependence on real or modeled atmospheric profiles and, therefore, to retrieve LST in a more operational way, different SC algorithms can be inferred from approximations of (1). Hence, an SC algorithm for L5B6 data was developed by Qin *et al.* [7]. This algorithm requires the knowledge of the atmospheric transmissivity (τ) and the atmospheric mean temperature $(T_{\rm a})$, which is something similar to have atmospheric profiles. For this reason, the authors used simulated data computed with LOWTRAN-7 code [8] to fit τ versus atmospheric water vapor content (w) and $T_{\rm a}$ versus near-surface air temperature (T_0) as input data. In this way, the algorithm uses w and T_0 as input data. However, relationships between τ and w depend on not well-defined "high" and "low" air temperature values, whereas relationships between $T_{\rm a}$ and T_0 are given for certain standard atmospheres.

To avoid the aforementioned problems, Jiménez-Muñoz and Sobrino [9] developed a generalized SC algorithm *a priori* applicable to any TIR channel with a bandwidth of around 1 μm. This algorithm was also adapted to L5B6 data in the cited reference and compared with the algorithm of Qin *et al.* in [10]. The basis of this algorithm relies in the estimation of the so-called atmospheric functions (AFs), which were assumed to be dependent only on w. Therefore, in terms of its practical application to Landsat-5 imagery, the main advantage is that only the knowledge of w is required. We will denote this algorithm as SC$^{\rm JM\&S}$.

It should be noted that all SC algorithms based on (1) require the additional knowledge of the land surface emissivity (LSE).

The purpose of this paper is to update the coefficients involved in the relationship between AFs and w for L5B6 data and also to extend the calculations to AFs for L4B6 and L7B6. In this way, an operative SC algorithm could be used to retrieve LST from the Landsat historical database and the new acquisitions in case of the program continuity. The problems of the LSE retrieval from Landsat data will not be addressed in this paper. The interested reader can consult, for example, [4], [10], and [11]. Problems related to the calibration of the Landsat thermal data will not be addressed in this paper either. More information about this issue can be found, for example, in [12] and [13].

II. Methodology

In this section, we provide a summary of the SC$^{\rm JM\&S}$ algorithm [9] in order to clarify to the reader about the results presented in the next sections. We also include a brief analysis of the bandpass effect, which regards to the difference between brightness temperatures derived by inversion of the Planck's law (monochromatic case) and brightness temperatures derived from band-averaged radiances. Moreover, we have included a description of the atmospheric radiosounding databases used in this paper.

A. SC Algorithm

SC$^{\rm JM\&S}$ algorithm retrieves LST $(T_{\rm s})$ using the following general equation:

$$T_{\rm s} = \gamma\left[\frac{1}{\varepsilon}(\psi_1 L_{\rm sen} + \psi_2) + \psi_3\right] + \delta \tag{3}$$

where ε is the surface emissivity; γ and δ are two parameters dependent on the Planck's function [see (4) and (5)]; and ψ_1, ψ_2, and ψ_3 are referred to as AFs [see (6)]. All the parameters involved in (3) are wavelength (or channel) dependent, but spectral notation will be omitted for simplicity. These parameters are given by

$$\gamma = \frac{1}{\beta} \quad \delta = -\frac{\alpha}{\beta} \tag{4}$$

$$\alpha = B(T_0)\left[1 - \frac{c_2}{T_0}\left(\frac{\lambda^4}{c_1}B(T_0) + \frac{1}{\lambda}\right)\right]$$

$$\beta = \frac{c_2 B(T_0)}{T_0^2}\left[\frac{\lambda^4 B(T_0)}{c_1} + \frac{1}{\lambda}\right] \tag{5}$$

$$\psi_1 = \frac{1}{\tau} \quad \psi_2 = -L^{\downarrow} - \frac{L^{\uparrow}}{\tau} \quad \psi_3 = L^{\downarrow}. \tag{6}$$

In (5), λ refers to the effective wavelength of the channel considered and T_0 is an approximated value to the surface temperature (not to be confused with air temperature). We will deal with these aspects in Section II-B. The practical approach proposed in the SC$^{\rm JM\&S}$ algorithm consists on the approximation of the AFs defined in (6) versus the atmospheric water vapor content from a polynomial (second degree) fit. In matrix notation, this approximation can be expressed as

$$\begin{bmatrix}\psi_1\\ \psi_2\\ \psi_3\end{bmatrix} = \begin{bmatrix}c_{11} & c_{12} & c_{13}\\ c_{21} & c_{22} & c_{23}\\ c_{31} & c_{32} & c_{33}\end{bmatrix}\begin{bmatrix}w^2\\ w\\ 1\end{bmatrix} \tag{7}$$

where coefficients c_{ij} are obtained by simulation. The following matrix coefficients were obtained for L5B6 data in [9]:

$$C = \begin{bmatrix}0.14714 & -0.15583 & 1.1234\\ -1.1836 & -0.37607 & -0.52894\\ -0.04554 & 1.8719 & -0.39071\end{bmatrix}. \tag{8}$$

Simulation procedure was performed with a set of 61 atmospheric soundings and MODTRAN 3.5 code to compute values of τ, $L^{\uparrow}$, and $L^{\downarrow}$. These atmospheric soundings carry certain w values which were computed using the LOWTRAN-7 code. In Section III, we provide updated coefficients using MODTRAN 4 computations for τ, $L^{\uparrow}$, and $L^{\downarrow}$ and also for w. The study will also be extended to L4B6 and L7B6 data.

1) Approximations for Gamma and Delta Parameters: Parameters γ and δ, defined in (4) and (5) and involved in LST retrieval from (3), explicitly depend on T_0 and $B(T_0)$. As discussed in [9], T_0 can be chosen as the at-sensor brightness temperature $T_{\rm sen}$ defined as $L_{\rm sen} \equiv B(T_{\rm sen})$. Therefore, $T_{\rm sen}$ can be obtained from inversion of Planck's law according to

$$T_{\rm sen} = \frac{c_2}{\lambda \ln\left(\frac{c_1}{\lambda^5 L_{\rm sen}} + 1\right)}. \tag{9}$$

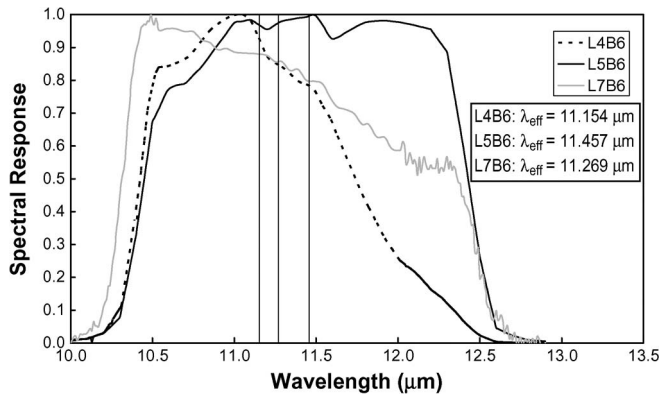

Fig. 1. Spectral responses and effective wavelengths ($\lambda_{\rm eff}$) for band 6 of Landsat-4 (L4B6), Landsat-5 (L5B6), and Landsat-7 (L7B6) platforms. Vertical lines are the position on the x-axis of $\lambda_{\rm eff}$.

In this way, γ and δ can be rewritten as presented in [10]

$$\gamma = \left\{ \frac{c_2 L_{\rm sen}}{T_{\rm sen}^2} \left[\frac{\lambda^4 L_{\rm sen}}{c_1} + \frac{1}{\lambda} \right] \right\}^{-1}$$
$$\delta = -\gamma L_{\rm sen} + T_{\rm sen}. \tag{10}$$

The parameter γ can also be expressed as

$$\gamma = \frac{T_{\rm sen}^2}{a_\gamma L_{\rm sen}^2 + b_\gamma L_{\rm sen}} \tag{11}$$

where

$$a_\gamma \equiv \frac{c_2 \lambda^4}{c_1}$$
$$b_\gamma \equiv \frac{c_2}{\lambda}. \tag{12}$$

It is easy to check that $a_\gamma \ll b_\gamma$ and also $a_\gamma L_{\rm sen}^2 \ll b_\gamma L_{\rm sen}$, so γ and δ can finally be easily obtained as

$$\gamma \approx \frac{T_{\rm sen}^2}{b_\gamma L_{\rm sen}}$$
$$\delta \approx T_{\rm sen} - \frac{T_{\rm sen}^2}{b_\gamma} \tag{13}$$

with b_γ equal to 1290 K, 1256 K, and 1277 K for L4B6, L5B6, and L7B6, respectively.

2) Effective Wavelength and Brightness Temperature Inversion: In previous expressions, the parameter λ is the effective wavelength of the sensor, which is defined as

$$\lambda_{\rm effective} = \frac{\int \lambda f_\lambda d\lambda}{\int f_\lambda d\lambda} \tag{14}$$

where f_λ is the filter function or spectral response for a certain sensor channel. Fig. 1 shows the spectral responses and the effective wavelengths for L4B6, L5B6, and L7B6.

Therefore, the computation of at-sensor brightness temperatures from the at-sensor registered radiance using (9) should employ effective wavelengths. The use of a single wavelength value to retrieve temperature from radiance in the case of a sensor with a certain channel width (sometimes referred in the literature as bandpass effects) has been revised by different authors [14]. A commonly used approximation of Planck's function specific to Landsat is given by [15]

$$T_{\rm sen} = \frac{K_2}{\ln\left(\frac{K_1}{L_{\rm sen}} + 1\right)} \tag{15}$$

where $K_1 = 671.62$ W $\cdot$ m^{-2} $\cdot$ sr^{-1} $\cdot$ μm^{-1} and $K_2 = 1284.30$ K for L4B6, $K_1 = 607.76$ W $\cdot$ m^{-2} $\cdot$ sr^{-1} $\cdot$ μm^{-1} and $K_2 = 1260.56$ K for L5B6, and $K_1 = 666.09$ W $\cdot$ m^{-2} $\cdot$ sr^{-1} $\cdot$ μm^{-1} and $K_2 = 1282.71$ K for L7B6. These constants were estimated to solve, in part, the problem of the bandpass effect. Mean differences between (9) and (15) for a range of temperatures between 270 K and 340 K have been found to be of -0.6 K for L4B6 and L5B6 and -0.3 K for L7B6. For example, note that in case of an error on LST of 1.5 K, square root sum of errors leads to 1.6 K or 1.5 K (i.e., $[1.5^2 + 0.6^2]^{1/2}$ or $[1.5^2 + 0.3^2]^{1/2}$), which is not a significant contribution. Since the SC algorithm presented here was developed from Planck's law and its derivatives, we will always employ the concept of effective wavelength.

B. Atmospheric Sounding Databases

In this section, we describe the five atmospheric sounding databases used to compute the AFs that will be presented later (see Section III-A). The atmospheric profiles of the different databases include values of altitude, pressure, temperature, and relative humidity for each layer. The rest of the values for the atmospheric constituents were retrieved from default values included in the appropriate MODTRAN standard atmosphere.

We have considered in this paper three thermodynamic initial guess retrieval (TIGR) databases described, for example, by Aires *et al.* [17]: 1) TIGR1, composed by 861 atmospheres [18]; 2) TIGR2, which is a revision of TIGR1 and is composed by 1761 atmospheres (assigned to the following model atmospheres: 322 tropical, 388 midlatitude summer, 354 midlatitude winter, 104 subartic summer, and 593 subartic winter) [19], [20]; and 3) TIGR3, an extended version of TIGR2 and composed by 2311 atmospheres (same as TIGR2 plus 550 atmospheres assigned to the tropical model) [21]. In fact, we have used TIGR2, TIGR3, and a selection of 61 atmospheres from TIGR1 (28 atmospheres assigned to the tropical model, 12 to the midlatitude summer model, 12 to the subartic winter, and 9 to the U.S. Standard). This reduced TIGR1 database was created by Sobrino *et al.* [22], and it has been used in numerous studies, including the development of the SC$^{\rm JM\&S}$ algorithm [9]. For simplicity, these databases will be referred by the number of atmospheres, i.e., TIGR61, TIGR1761, and TIGR2311.

In addition to the TIGR databases, we have also considered the SAFREE database presented in [23]. This database includes 402 cloud-free and latitude equally distributed profiles representative of the world ocean. It has been made from four main radiosounding sources: TIGR2, TIGR3, and radiosoundings from Meteo France and the Norwegian Meteorological service. Despite the fact that SAFREE was originally developed for maritime conditions, we have used it also indistinctly over land.

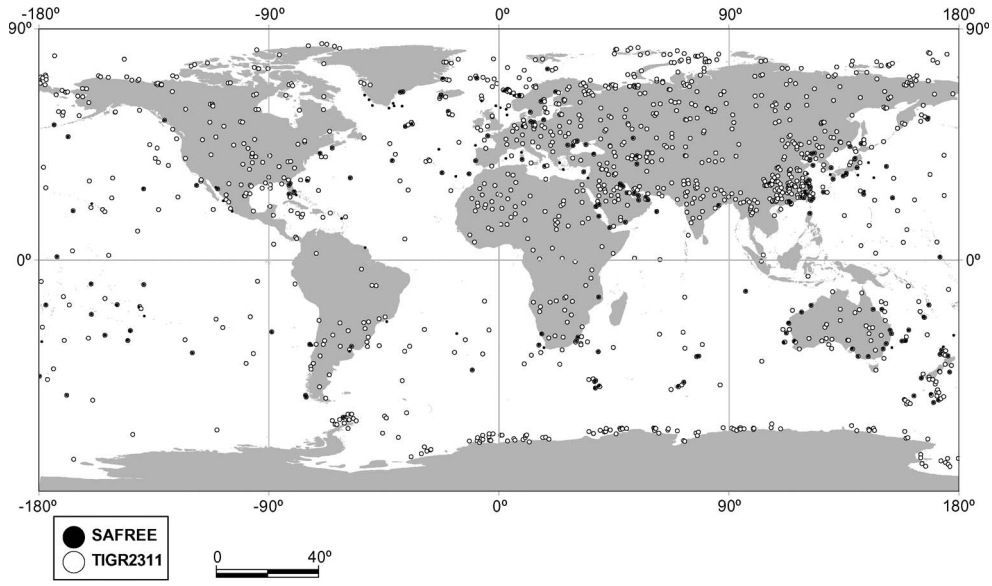

Fig. 2. Spatial distribution of the atmospheric profiles included in the SAFREE and TIGR databases.

TABLE I
ATMOSPHERIC SOUNDING DATABASES CONSIDERED IN THE SIMULATION PROCEDURE USING MODTRAN RADIATIVE TRANSFER CODE. ABBREVIATIONS FOR MODEL ATMOSPHERES: TRO = TROPICAL, MLS = MIDLATITUDE SUMMER, MLW = MIDLATITUDE WINTER, SAS = SUBARTIC SUMMER, SAW = SUBARTIC WINTER, AND USS = U.S. STANDARD

Database notation	Original database	Number of atmospheric profiles	Model atmospheres
TIGR61	TIGR1	61	28 TRO 12 MLS 12 SAW 9 USS
TIGR1761	TIGR2	1761	322 TRO 388 MLS 354 MLW 104 SAS 593 SAW
TIGR2311	TIGR3	2311	872 TRO 388 MLS 354 MLW 104 SAS 593 SAW
SAFREE402	SAFREE	402	Not specified (maritime conditions)
STD66	Standard atmospheres included in MODTRAN	66	11 TRO 11MLS 11 MLW 11 SAS 11 SAW 11 USS

This database will be denoted as SAFREE402. Fig. 2 shows the spatial distribution of the atmospheric profiles included in the TIGR and SAFREE databases.

Finally, we have constructed an additional database by considering the six standard (std) atmospheric profiles (tropical, midlatitude summer, midlatitude winter, subartic summer, subartic winter, and U.S. Standard) included in the MODTRAN code and a scaling water vapor factor from 0.5 to 1.5 in steps of 0.1. This leads to a total amount of 66 atmospheres, so we denote this database as STD66. The atmospheric database characteristics are summarized in Table I.

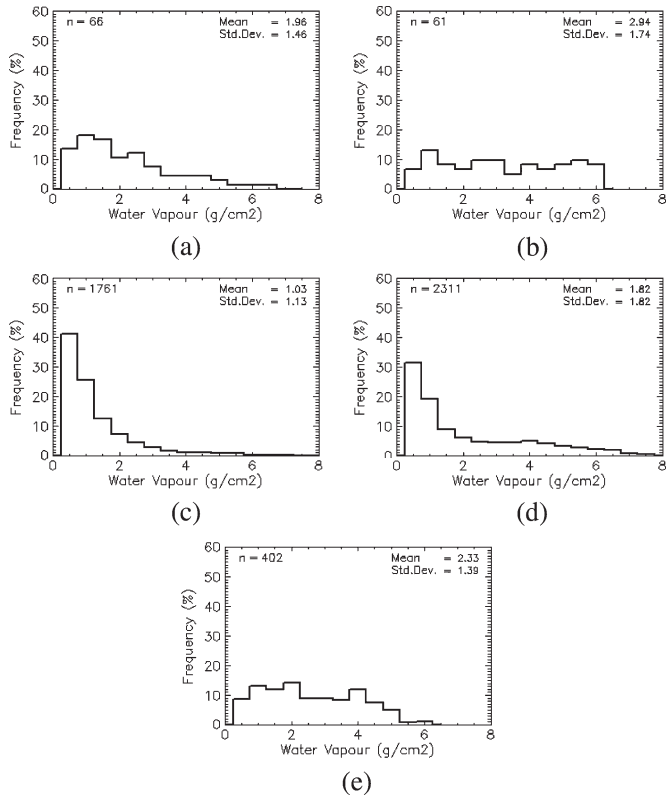

Fig. 3. Atmospheric water vapor content histogram for the different atmospheric sounding databases employed: (a) STD66, (b) TIGR61, (c) TIGR1761, (d) TIGR2311, and (e) SAFREE402.

Fig. 3 shows the histogram in terms of the atmospheric water vapor content distribution for each database. Hence, TIGR1761 and TIGR2311 are centered at low w values, around 1 g/cm^2. The rest of databases are not clearly centered at any particular

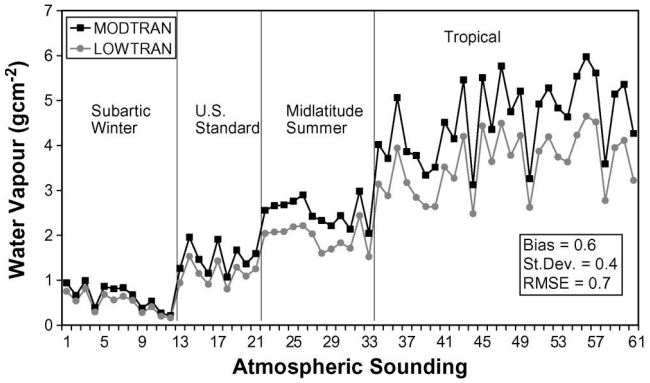

Fig. 4. Output atmospheric water vapor content from LOWTRAN and MODTRAN for each atmospheric profile included in the TIGR61 database. Model atmosphere in which each atmospheric sounding is assigned is also shown.

w value. TIGR61 seems to be the better distributed database in terms of water vapor.

As commented in Section II-A, the first version of the AFs involved in the $\text{SC}^{\text{JM\&S}}$ algorithm was retrieved from LOWTRAN calculations for the total atmospheric water vapor content but from MODTRAN calculations for atmospheric transmissivity and atmospheric radiances. This was done because in older versions of MODTRAN, w values were provided in units of g $\cdot$ cm^{-2} only when it was executed in LOWTRAN mode. Newer versions of MODTRAN, such as version 4, provide w values in units of atm $\cdot$ cm and g $\cdot$ cm^{-2}, so in this paper, AFs have been computed only using MODTRAN calculations. Significant differences between LOWTRAN and MODTRAN estimations of w values have been found, and they are reported in Fig. 4. A root mean square error (rmse) value of 0.7 g $\cdot$ cm^{-2} (taking w obtained by MODTRAN as the reference) has been obtained in the case of TIGR61. These differences can be higher than 1 g $\cdot$ cm^{-2} for high w values. In the next section, we present the revised coefficients obtained from TIGR61 using only MODTRAN calculations.

III. Results

In this section, we provide recalculated coefficients for the AFs of L5B6 and also the first calculations for L4B6 and L7B6. These calculations have been performed using simulated data extracted from different atmospheric sounding databases (see Section II-B) and MODTRAN-4 code [16]. Final results on LST have been tested using independent simulated data. An effort has been made to also include a test from Landsat imagery and ground data. However, the authors do not have a complete database of imagery and measurements to ensure a complete validation. A "ground-truth" LST map over an agricultural area obtained from inversion of RTE and an atmospheric sounding launched *in situ* has been used instead, as will be explained in Section III-C. It is worth to remark that the $\text{SC}^{\text{JM\&S}}$ algorithm was previously validated with ground-based measurements in [9] and tested using simulated and Landsat-5 TM data in [10].

A. AFs

Atmospheric profiles included in the different databases have been introduced in the MODTRAN-4 code to produce spectral values of τ, $L^{\uparrow}$, and $L^{\downarrow}$. Band-averaged (effective) values were retrieved using spectral responses (see Fig. 1) and (14), in which λ must be replaced by the parameter considered (τ, $L^{\uparrow}$, or $L^{\downarrow}$). Then, AFs were calculated from (6) and fitted against w. The coefficients obtained for each AF, database, and sensor are given in Table II, in which matrix notation has been considered as presented in Section II-A.

Coefficients of determination (r^2) and standard error of estimations (σ) obtained in the statistical fits of AFs were also calculated, but they are not shown in Table II. Values of r^2 were typically > 0.96, which indicated a good correlation between AFs and w. Values of σ for the AFs do not provide useful information *per se*. For this reason, LST has been retrieved from

TABLE II
Coefficients for the AFs Following Matrix Notation Expressed in (7). Values Have Been Obtained Using Different Atmospheric Sounding Databases for Band 6 of Landsat-4, Landsat-5, and Landsat-7 Platforms

Database	Sensor	Cij	i=1	i=2	i=3
STD66	L4B6	j=1	0.08767	-0.09665	1.09023
		j=2	-0.70317	-0.61239	-0.12239
		j=3	-0.02518	1.51142	-0.48763
TIGR61	L4B6	j=1	0.07247	-0.06968	1.0788
		j=2	-0.60283	-0.68176	-0.13311
		j=3	-0.01999	1.43469	-0.46157
TIGR1761	L4B6	j=1	0.06240	0.00373	1.02425
		j=2	-0.52383	-1.19361	0.12908
		j=3	-0.00960	1.33393	-0.25891
TIGR2311	L4B6	j=1	0.06674	-0.03447	1.04483
		j=2	-0.50095	-1.15652	0.09812
		j=3	-0.04732	1.50453	-0.34405
SAFREE402	L4B6	j=1	0.04399	0.05765	1.00499
		j=2	-0.32119	-2.09785	0.59914
		j=3	-0.0554	1.67195	-0.49334
STD66	L5B6	j=1	0.1062	-0.13016	1.11576
		j=2	-0.81365	-0.47596	-0.29139
		j=3	-0.04421	1.61507	-0.48656
TIGR61	L5B6	j=1	0.08735	-0.09553	1.10188
		j=2	-0.69188	-0.58185	-0.29887
		j=3	-0.03724	1.53065	-0.45476
TIGR1761	L5B6	j=1	0.07518	-0.00492	1.03189
		j=2	-0.59600	-1.22554	0.08104
		j=3	-0.02767	1.43740	-0.25844
TIGR2311	L5B6	j=1	0.08158	-0.05707	1.05991
		j=2	-0.58853	-1.08536	-0.00448
		j=3	-0.06201	1.59086	-0.33513
SAFREE402	L5B6	j=1	0.05261	0.05933	1.01123
		j=2	-0.36368	-2.20569	0.55116
		j=3	-0.07237	1.76355	-0.47457
STD66	L7B6	j=1	0.09172	-0.09894	1.09659
		j=2	-0.71656	-0.64218	-0.17183
		j=3	-0.03503	1.54063	-0.46434
TIGR61	L7B6	j=1	0.07593	-0.07132	1.08565
		j=2	-0.61438	-0.70916	-0.19379
		j=3	-0.02892	1.46051	-0.43199
TIGR1761	L7B6	j=1	0.06518	0.00683	1.02717
		j=2	-0.53003	-1.25866	0.10490
		j=3	-0.01965	1.36947	-0.24310
TIGR2311	L7B6	j=1	0.06982	-0.03366	1.04896
		j=2	-0.51041	-1.20026	0.06297
		j=3	-0.05457	1.52631	-0.32136
SAFREE402	L7B6	j=1	0.04597	0.06269	1.00818
		j=2	-0.32297	-2.16801	0.55698
		j=3	-0.06397	1.69324	-0.45747

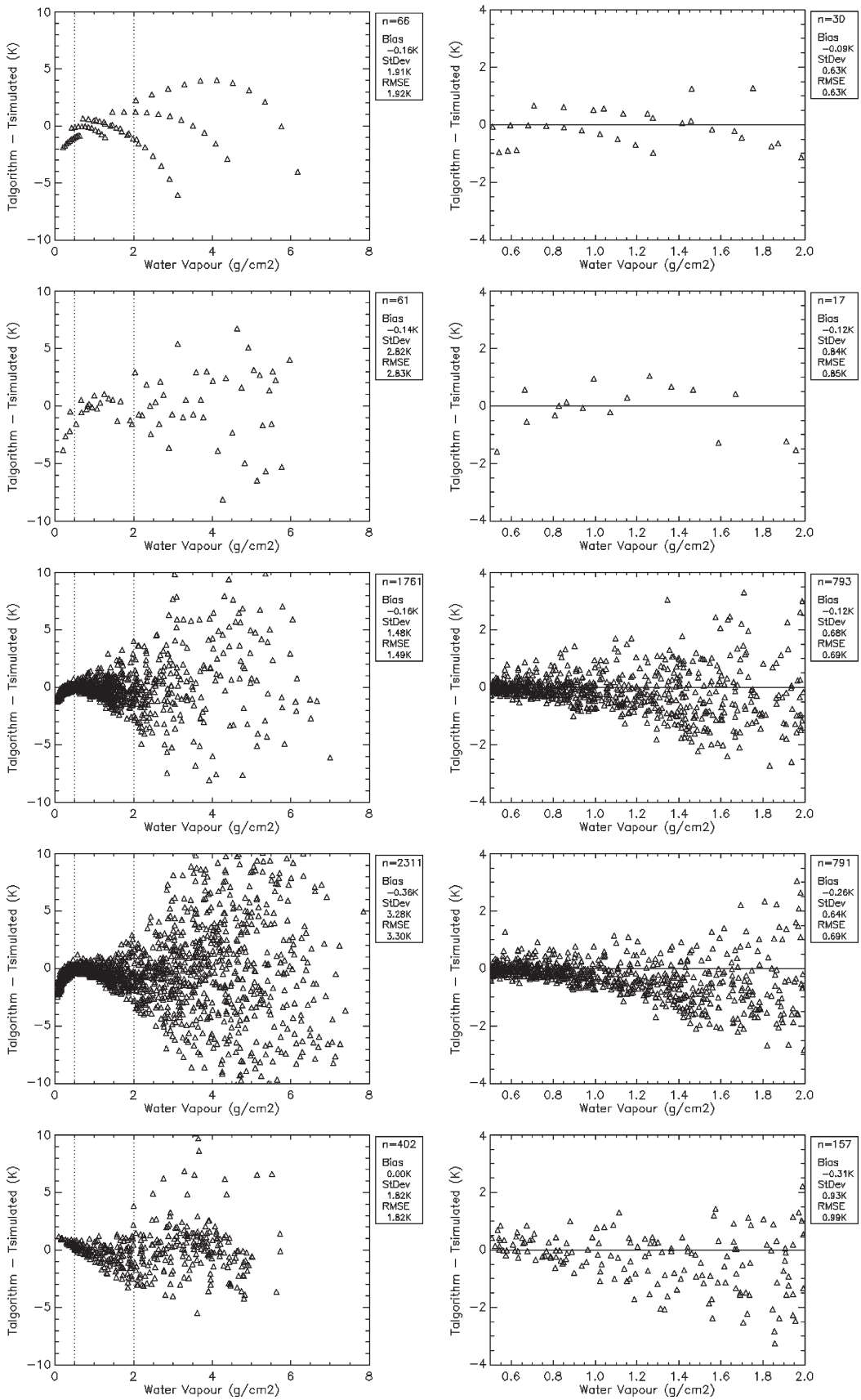

Fig. 5. Test of the SC algorithm using the same simulated data than used for retrieving the AFs. Plots show the difference between the LST retrieved with the SC algorithm ($T_{\mathrm{algorithm}}$) and the one included in the simulated database ($T_{\mathrm{simulated}}$) (left column) for the whole range of water vapor values and (right column) only for the range between 0.5 and 2 g $\cdot$ cm^{-2}. Values of bias, standard deviation, and rmse are also given. Surface emissivity has been assumed to be 1.0. From top to bottom, plots correspond to STD66, TIGR61, TIGR1761, TIGR2311, and SAFREE402 databases.

(3) using AFs computed with the same simulated data, and then compared to LST extracted from the atmospheric soundings (temperature at first level). Since emissivity is assumed to be known, a value of 1.0 has been considered (same results are also obtained for emissivity values different to the unity). This procedure provides an idea of the σ value in terms of temperature and not in terms of AFs. Fig. 5 shows the results obtained for L5B6. Plots included in Fig. 5 represent the difference between LST retrieved with the SC$^{\mathrm{JM\&S}}$ algorithm and LST simulated versus the atmospheric water vapor content. These plots clearly show that poor results are obtained for very low w values ($w < 0.5$ g $\cdot$ cm^{-2}), and overall for high w values, $w > 3$ g $\cdot$ cm^{-2}. There is also a "transition zone" between 2 and 3 g $\cdot$ cm^{-2}, in which the algorithm can provide acceptable results in some cases. For this reason, we have also plotted in Fig. 5 the results obtained only for w values between 0.5 and 2 g $\cdot$ cm^{-2}, which can be considered the range of good performance for the algorithm. When results are focused in this range of w values, rmse < 0.7 K are obtained for all the databases, except for the SAFREE one, with rmse < 1 K. Note that when the full range of w values is considered, STD66, TIGR1761, and SAFREE402 still provide acceptable results, with rmse < 2 K, whereas TIGR61 and TIGR2311 provide rmse $\sim$3 K.

B. Algorithm Testing Using Independent Simulated Data

In the previous section, we provided a test for the SC algorithm using the same simulated data than used to retrieve the coefficients for the AFs, which indicates expected errors only due to the statistical fit between AFs and w, i.e., something similar to a standard error of estimation. In this section, we show results obtained when the SC$^{\mathrm{JM\&S}}$ algorithm is applied to an independent simulated database. For this purpose, we will use AFs calculated from one atmospheric database, and we will apply the algorithm to the rest of the atmospheric databases. In this case, surface emissivities involved in (3) have been obtained from the ASTER spectral library (108 samples used in [24]). The results obtained in this test for L4B6, L5B6, and L7B6 are presented in Table III. Note that TIGR1761, TIGR2311, and SAFREE402 have not been intercompared because they share some atmospheric profiles, which could lead to an underestimation of the rmse.

According to the results presented in Table III, similar conclusions than in the previous section can be extracted, i.e., SC$^{\mathrm{JM\&S}}$ algorithm shows a good performance for w values between 0.5 and 2 g $\cdot$ cm^{-2}, with rmse values below 1 K, except for the SAFREE database, with rmse values between 1.3 K and 1.6 K. This is probably due to the fact that the SAFREE database was designed only for maritime conditions. Acceptable results are obtained in some cases for the full range of w values. For example, when AFs are retrieved with the three TIGR databases and the SC$^{\mathrm{JM\&S}}$ is compared to the STD66 database, rmse values are below 2 K. AFs retrieved from TIGR2311 and SC$^{\mathrm{JM\&S}}$ compared to TIGR1761 also provide satisfactory results for the full range of w values, with an rmse of 1.5 K.

TABLE III
TEST OF THE SC ALGORITHM USING INDEPENDENT SIMULATED DATA. AFS ARE RETRIEVED FROM ONE DATABASE, AND SC ALGORITHM IS TESTED WITH THE REST OF THE DATABASES CONSIDERED IN THIS PAPER. RMSE IS THE ROOT MEAN SQUARE ERROR

Database AFs	Database Test	w Range (gcm^{-2})	Bias (K)	St.Dev. (K)	RMSE (K)
STD66	TIGR61	All	0.8	3.6	3.7
	TIGR61	0.5<w<2	0.0	0.9	0.9
	TIGR1761	All	-0.9	2.2	2.4
	TIGR1761	0.5<w<2	0.0	0.6	0.6
	SAFREE402	All	1.9	2.7	3.3
	SAFREE402	0.5<w<2	0.5	0.7	0.9
	TIGR2311	All	-0.7	4.3	4.3
	TIGR2311	0.5<w<2	0.0	0.7	0.7
TIGR61	STD66	All	-0.6	1.9	2.0
	STD66	0.5<w<2	-0.3	0.7	0.7
	TIGR1761	All	-1.3	2.1	2.5
	TIGR1761	0.5<w<2	-0.3	0.7	0.7
	SAFREE402	All	1.2	2.1	2.4
	SAFREE402	0.5<w<2	0.4	0.7	0.8
	TIGR2311	All	-1.4	3.9	4.1
	TIGR2311	0.5<w<2	-0.3	0.7	0.8
TIGR1761	STD66	All	-0.1	1.9	1.9
	STD66	0.5<w<2	-0.1	0.7	0.7
	TIGR61	All	0.7	3.1	3.2
	TIGR61	0.5<w<2	-0.1	1.0	1.0
TIGR2311	STD66	All	-0.4	1.7	1.8
	STD66	0.5<w<2	-0.4	0.6	0.7
	TIGR61	All	0.5	3.0	3.1
	TIGR61	0.5<w<2	-0.3	0.9	1.0
SAFREE402	STD66	All	-1.5	2.4	2.8
	STD66	0.5<w<2	-0.9	1.0	1.3
	TIGR61	All	-1.6	3.0	3.4
	TIGR61	0.5<w<2	-0.9	1.4	1.6

C. Algorithm Testing Using Satellite Data

As has been commented before, the authors do not have a complete Landsat imagery database in coincidence with ground-based LSTs to provide a complete validation. Instead, we provide in this section a brief analysis using one Landsat-5 image acquired on July 13, 2005 over the agricultural area of Barrax (Albacete, Spain, 39.05° N, 2.1° W, 700 m) in the framework of the SEN2FLEX field campaign [25]. Landsat image was resized to 393 $\times$ 391 pixels ($\sim$138 km^2), which includes the study area under clear-sky conditions. Ground-based measurements were collected to validate high-resolution airborne data, with pixel size < 5 m, so these plots are not valid at Landsat-5 scale (pixel size of 120 m). For this reason, we have obtained an LST image by inversion of the RTE (1), where atmospheric parameters τ, $L^{\uparrow}$, and $L^{\downarrow}$ were obtained from MODTRAN, and the atmospheric sounding launched

in situ at 10:48 GMT, close to the Landsat overpass time (10:31 GMT). LSE was obtained using the simplified normalized difference vegetation index (SNDVI) method [11]

$$\varepsilon = \varepsilon_{\rm s}(1 - {\rm FVC}) + \varepsilon_{\rm v}{\rm FVC} \tag{16}$$

where $\varepsilon_{\rm s}$ and $\varepsilon_{\rm v}$ refer to soil and vegetation emissivities, assumed to be of 0.97 and 0.99, respectively, for the Barrax area. Fractional vegetation cover (FVC) can be retrieved from NDVI according to Carlson and Ripley [26]

$${\rm FVC} = \left[\frac{{\rm NDVI} - {\rm NDVI_s}}{{\rm NDVI_v} - {\rm NDVI_s}}\right]^2 \tag{17}$$

where $\rm NDVI_s$ and $\rm NDVI_v$ refer to soil and vegetation NDVI, with respective values extracted from the NDVI histogram of 0.18 and 0.85. NDVI was computed using reflectances at Landsat bands 3 and 4, atmospherically corrected using the algorithm developed by Guanter *et al.* [27], and adapted to Landsat characteristics. For those pixels where NDVI $<$ $\rm NDVI_s$, FVC is set to zero, whereas for pixels with NDVI $>$ $\rm NDVI_v$, FVC is set to one.

The LST image retrieved using the aforementioned procedure has been considered as a "ground-truth" map (denoted as RTE_truth), and LST retrievals considering different cases have been compared to it. The different ways cases considered in the LST retrieval are as follows.

1) Use the RTE, in which atmospheric parameters (τ, $L^{\uparrow}$, and $L^{\downarrow}$) are retrieved using the atmospheric correction parameter calculator (ACPC) developed in [5] and [6] (denoted as RTE_ACPC).
2) Use the $\rm SC^{JM\&S}$ algorithm, in which AFs are calculated directly from (6) and using values for the atmospheric parameters (τ, $L^{\uparrow}$, and $L^{\downarrow}$) obtained from the atmospheric sounding and MODTRAN (denoted as SC_theory).
3) Use the $\rm SC^{JM\&S}$ algorithm, in which AFs are calculated using the coefficients obtained with the TIGR61 database and the water vapor value extracted from the atmospheric sounding (denoted as SC_w).

Values of the atmospheric parameters extracted from the atmospheric sounding and from the ACPC are given in Table IV. RTE_truth has been subtracted to LST images obtained in the three different cases. The results are included in Table V, which shows that RTE_ACPC and SC_w are clearly biased in 1.5 K, with maximum differences up to 2 K. SC_theory provided almost the same results than RTE_truth, with a bias below 0.2 K. This low bias suggests that the "theoretical" approximations involved in the $\rm SC^{JM\&S}$ algorithm are satisfactory, and as it is expected, accuracy is lost due to the strong approximation of the AFs versus only a single atmospheric parameter as the water vapor content. The significant bias obtained with the RTE_ACPC suggests that atmospheric corrections based on NCEP models can be very useful at global scales, but its accuracy at regional scales and for a particular case is uncertain.

We have also checked if surface emissivity estimation from FVC values according to (16) and (17) is sensitive to the atmospheric correction for Landsat bands 3 and 4. For this purpose, we have estimated FVC from NDVI computed using digital counts (DCs). In this case, values of $\rm NDVI_s = 0.02$ and $\rm NDVI_v = 0.61$ were found. FVC values obtained from NDVI computed in DCs were used to obtain surface emissivity, which was used to retrieve LST from inversion of RTE. Comparison against RTE_truth provided a mean difference (bias) of -0.1 K and standard deviation of 0.3 K. A difference of -0.005 K was found for 60.5% of the pixels. This result suggests that in this particular case, it is not totally necessary to perform radiometric and atmospheric correction to retrieve FVC from a scaled NDVI as proposed in (17), at least in terms of LST retrieval using surface emissivities estimated from (16).

TABLE IV
VALUES OF ATMOSPHERIC PARAMETERS OBTAINED FROM THE ATMOSPHERIC SOUNDING LAUNCHED ON JULY 13, 2005 AT 10:48 GMT OVER THE BARRAX AREA AND THE ONES EXTRACTED FROM THE ACPC

Parameter	Atmospheric Sounding	ACPC
Transmissivity (τ) [unitless]	0.82	0.76
Up-welling radiance ($L^{\uparrow}$) [$\rm wm^{-2}sr^{-1}\mu m^{-1}$]	1.43	1.86
Down-welling radiance ($L^{\downarrow}$) [$\rm wm^{-2}sr^{-1}\mu m^{-1}$]	2.15	3.07
Water vapour (w) [$\rm gcm^{-2}$]	1.58	2.10

TABLE V
VALUES OF THE DIFFERENCE BETWEEN THREE DIFFERENT RETRIEVED LST IMAGES AND THE "GROUND-TRUTH" LST IMAGE OBTAINED FROM INVERSION OF THE RTE USING AN ATMOSPHERIC SOUNDING AND MODTRAN CODE. LST IMAGES HAVE BEEN RETRIEVED USING RTE AND ATMOSPHERIC PARAMETERS FROM THE ACPC (RTE_ACPC), USING THE SC ALGORITHM WITH AFS DIRECTLY CALCULATED FROM ATMOSPHERIC PARAMETERS EXTRACTED FROM THE ATMOSPHERIC SOUNDING (SC_THEORY), AND USING THE SC ALGORITHM WITH THE EMPIRICAL AFS OBTAINED FROM THE TIGR61 DATABASE (SC_W)

Algorithm	Maximum	Minimum	Bias	St. Dev	RMSE
RTE_ACPC	2.1	0.5	1.5	0.4	1.6
SC_theory	0.3	0.02	0.17	0.07	0.18
SC_w	2.1	1.1	1.5	0.2	1.5

D. Implementation of the SC Algorithm

Once the $\rm SC^{JM\&S}$ algorithm has been revised and updated, we provided in this section a guide to implement the algorithm. Hence, to apply the SC algorithm to Landsat imagery, one can use the following procedures.

1) Convert DCs in band 6 into at-sensor thermal radiances ($L_{\rm sen}$) using the linear relationship $L_{\rm sen} = {\rm gain} \times {\rm DC} + {\rm offset}$.
2) Convert to brightness temperatures using (9) and effective wavelengths presented in Fig. 1.
3) Calculate γ and δ parameters using the simplified expression given in (13). Original expression given in (10) can also be used.
4) Select appropriate coefficients for the AFs, ψ_1, ψ_2, and ψ_3, according to Table II. One can select, for example, coefficients obtained from TIGR61 database, composed by a reduced set of atmospheric profiles representative at

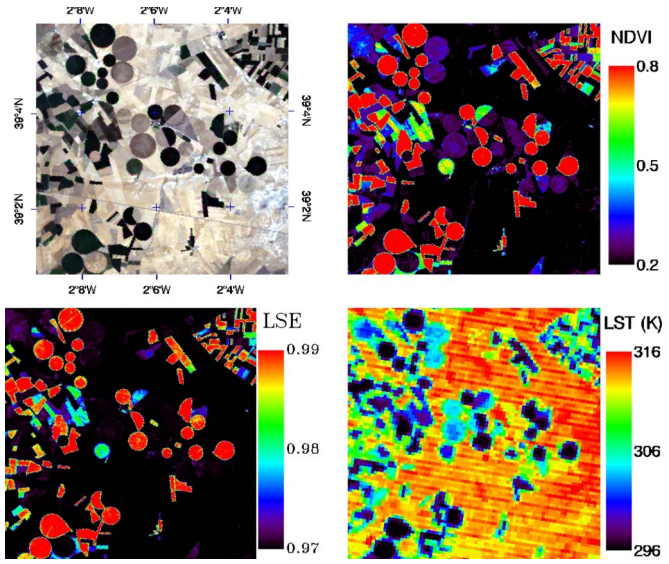

Fig. 6. Example of LST map obtained from Landsat-5 data using the SC algorithm revised in this paper. Index map constructed from an RGB composition (bands 3, 2, and 1), NDVI, and LSE maps are also shown. Landsat image was acquired on July 13, 2005 over the agricultural area of Barrax (Albacete, Spain).

world-wide scale. However, if the study area is located in high latitudes usually with a low w content, TIGR1761 should be selected, since it is more suitable for lower w. For open water or coastal areas, SAFREE402 database could be used instead.

5) Once the coefficients (c_{ij}) for the AFs have been selected, select an atmospheric water vapor content value (w) and calculate them from (7). Water vapor values can be obtained, for example, from ground-based measurements, atmospheric soundings, or MODIS products (MOD05).
6) Estimate LSE (ε). Selection of the appropriate method for ε retrieval relies on the user criteria. In Section III-D, we used a simple approximation between ε and FVC, referred to as SNDVI method in [11].
7) At this stage, once $L_{\rm sen}$, γ, δ, ψ_1, ψ_2, ψ_3, and ε have been calculated, LST is finally retrieved using (3).

Fig. 6 shows an example of the LST map obtained using the SC$^{\rm JM\&S}$ algorithm from the Landsat-5 data discussed in Section III-D.

E. Feasibility of Using an LUT

We would like to emphasize that the SC$^{\rm JM\&S}$ algorithm does not pretend to be more accurate than other SC algorithms but to be an operational algorithm with minimum input data requirements (only ε and w). As was discussed in Section II-B, coefficients for AFs depend on the atmospheric sounding database used or, in other words, depend on the mean atmospheric water vapor content of these databases. Therefore, LST retrievals will depend also on the atmospheric sounding databases used to retrieve the AFs. In addition, SC algorithms provide poor results for high w values (typically $w > 3$ g $\cdot$ cm^{-2}), which indicates that relationships between atmospheric parameters (τ, $L^{\uparrow}$, $L^{\downarrow}$) and water vapor are not satisfactory for a full range of w values. This fact suggests that coefficients could be calculated

TABLE VI
SAME AS TABLE V, BUT USING LST IMAGES RETRIEVED FROM INVERSION OF THE RTE AND AN LUT OF ATMOSPHERIC PARAMETERS (RTE_LUT) AND USING THE SC ALGORITHM AND AN LUTOF AFS (SC_LUT)

Algorithm	Maximum	Minimum	Bias	St. Dev	RMSE
RTE_LUT	0.8	0.7	0.719	0.016	0.7
SC_LUT	1.0	0.8	0.92	0.06	0.9

for different ranges of w values. For example, two different ranges were considered by Qin *et al.* [7], such as 0.4–1.6 and 1.6–3 g $\cdot$ cm^{-2}. Narrower ranges could also be considered to improve the estimation of atmospheric parameters from w values. Another possibility is to build a lookup table (LUT) and then interpolate according to the w value. This option has also been explored for the SC$^{\rm JM\&S}$ algorithm. For this purpose, the STD66 database has been used, since it is composed by different standard atmospheres but scaled for a full range of w values. LUT has been constructed for the AFs. Then, according to the most appropriate standard atmosphere for the acquired Landsat image and the w value, AFs are interpolated. To compare results, an LUT in terms of τ, $L^{\uparrow}$, and $L^{\downarrow}$ instead of AFs has also been constructed. The results obtained in the comparison against the "ground-truth" map discussed in Section III-D are presented in Table VI. Note that by using an LUT, the SC$^{\rm JM\&S}$ algorithm decreases the error from 1.5 (see Table V) to 0.9 K. This error is similar to the one obtained when using the RTE and the LUT (0.7 K). Note also that these errors are also lower than the one obtained with the RTE and the ACPC. We would like to emphasize that, as it is expected, the use of an LUT provides more accurate results than using statistical fits for the AFs versus w, but at the same time, the use of an LUT prevents the user to apply an operational algorithm easily implemented following the guidelines presented in Section III-E.

IV. SUMMARY AND CONCLUSION

SC algorithms are the unique algorithms for LST retrieval that can be applied to sensors with only one thermal channel, which is the case of the sensors onboard the Landsat platforms. Inversion of the RTE is *a priori* the best option for LST retrieval from one thermal band, since it does not involve additional approximations. However, this technique requires an accurate knowledge of atmospheric parameters such as transmissivity and atmospheric upwelling and downwelling radiances, which is not always possible. In order to solve this problem, these atmospheric parameters are fitted versus more accessible parameters such as atmospheric water vapor content, air temperature, etc. However, these relationships involve a strong approximation, which implies that they are not valid for a full range of w values but only for low/moderate w values $(w < 3$ g $\cdot$ cm$^{-2})$. Inaccuracies can also be found for very low w values $(w < 0.5$ g $\cdot$ cm$^{-2})$, which indicates that the error introduced in the atmospheric correction procedure is higher than if no atmospheric correction is performed, due to the almost negligible atmospheric effect at this low w values. In these cases, only an emissivity correction as proposed by Artis and Carnahan [28] could be considered. In this paper, we have

revised and updated in the case of Landsat-5 and extended to Landsat-4 and Landsat-7 platforms the SC algorithm developed by Jimenez-Muñoz and Sobrino [9], denoted throughout the paper as $\mathrm{SC}^{\mathrm{JM\&S}}$. In this way, LST could be retrieved from historical Landsat imagery databases. The algorithm relies in the concept of AFs, which are empirically expressed in terms only of water vapor content to minimize input data requirements. It is difficult to establish fixed criteria in order to select the atmospheric database (STD, TIGR, SAFREE, or others) needed to compute the AFs, but the knowledge of w ranges in the test area can help in selecting the appropriate database. For instance, in the case of TIGR61 database, its w range is well balanced, and it could be used as a global database. However, if the study area is located at high latitudes usually with a low w content, TIGR1761 database should be more suitable. When *in situ* measurements of surface temperatures are available for a set of images, one can apply the SC algorithm using all the atmospheric databases and then select for the complete imagery data set that atmospheric database for which the best results in the validation were obtained.

$\mathrm{SC}^{\mathrm{JM\&S}}$ is totally operational, and it can be adapted to any thermal band. Expected errors are between 1 and 2 K for w values between 0.5 and 2 $\mathrm{g \cdot cm^{-2}}$. In one particular case, with $w = 1.58$ $\mathrm{g \cdot cm^{-2}}$, the algorithm provided the same accuracy than inversion of RTE using atmospheric data extracted from NCEP models. Note that accurate LSTs for a wider range of w values can be obtained using an LUT, but this option prevents the reader to apply the algorithm by himself to its particular Landsat imagery.

The authors are working on the application of the SC algorithm to a long series of Landsat imagery over Catalonia (north–east of the Iberian Peninsula), which will illustrate better the performance of the algorithm.

ACKNOWLEDGMENT

The authors would like to thank C. François and P. Leborgne (Météo-France) for providing the SAFREE database, and B. Sebag and C. Crevoisier from the Laboratoire de Météorologie Dynamique/Groupe Analyse du Rayonnement Atmosphérique of the Ecole Polytechnique (Paris, France) for providing the TIGR-3 database and for the help in the database conversion to MODTRAN format. The authors would also like to thank L. Guanter (GeoForschungsZentrum Potsdam, Germany) who processed the atmospheric correction of the Landsat image.

REFERENCES

[1] D. A. Quattrochi and J. C. Luvall, "Thermal infrared remote sensing for analysis of landscape ecological processes: Methods and applications," *Landsc. Ecol.*, vol. 14, no. 6, pp. 577–598, Dec. 1999.

[2] D. A. Quattrochi and J. C. Luvall, *Thermal Remote Sensing in Land Surface Processes*. Boca Raton, FL: CRC Press, 2004, p. 440.

[3] S. J. Hook, G. Chander, J. A. Barsi, R. E. Alley, A. Abtahi, F. D. Palluconi, B. L. Markham, R. C. Richards, S. G. Schladow, and D. L. Helder, "In-flight validation and recovery of water surface temperature with Landsat-5 thermal infrared data using an automated high-altitude lake validation site at Lake Tahoe," *IEEE Trans. Geosci. Remote Sens.*, vol. 42, no. 12, pp. 2767–2776, Dec. 2004.

[4] F. Li, T. J. Jackson, W. P. Kustas, T. J. Schmugge, A. N. French, M. H. Cosh, and R. Bindlish, "Deriving land surface temperature from Landsat 5 and 7 during SMEX02/SMACEX," *Remote Sens. Environ.*, vol. 92, no. 4, pp. 521–534, Sep. 2004.

[5] J. A. Barsi, J. L. Barker, and J. R. Schott, "An atmospheric correction parameter calculator for a single thermal band earth-sensing instrument," in *Proc. IEEE IGARSS*, Toulouse, France, 2003, pp. 3014–3016.

[6] J. A. Barsi, J. R. Schott, F. D. Palluconi, and S. J. Hook, "Validation of a web-based atmospheric correction tool for single thermal band instruments," in *Proc. SPIE*, Bellingham, WA, 2005, vol. 5882.

[7] Z. Qin, A. Karnieli, and P. Berliner, "A mono-window algorithm for retrieving land surface temperature from Landsat TM data and its application to the Israel-Egypt border region," *Int. J. Remote Sens.*, vol. 22, no. 18, pp. 3719–3746, 2001.

[8] F. X. Kneizys, E. P. Shettle, L. W. Abreu, G. P. Anderson, J. H. Chetwynd, W. O. Gallery, J. E. A. Selby, and S. A. Clough, "Users guide to LOWTRAN-7," Opt./Infrared Technol. Division, US Air Force Geophys. Lab., Hanscom Air Force Base, Hanscom AFB, MA, Tech. Rep. AFGL-TR-88-0177, 1988.

[9] J. C. Jiménez-Muñoz and J. A. Sobrino, "A generalized single-channel method for retrieving land surface temperature from remote sensing data," *J. Geophys. Res.*, vol. 108, no. D22, p. 4688, Nov. 2003. DOI:10.1029/2003JD003480.

[10] J. A. Sobrino, J. C. Jiménez-Muñoz, and L. Paolini, "Land surface temperature retrieval from LANDSAT TM 5," *Remote Sens. Environ.*, vol. 90, no. 4, pp. 434–440, Apr. 2004.

[11] J. A. Sobrino, J. C. Jiménez-Muñoz, G. Sòria, M. Romaguera, L. Guanter, J. Moreno, A. Plaza, and P. Martínez, "Land surface emissivity retrieval from different VNIR and TIR sensors," *IEEE Trans. Geosci. Remote Sens.*, vol. 48, no. 2, pp. 316–327, Feb. 2008.

[12] J. R. Schott, J. A. Barsi, B. L. Nordgren, N. G. Raqueño, and D. de Alwis, "Calibration of Landsat thermal data and application to water resource studies," *Remote Sens. Environ.*, vol. 78, no. 1/2, pp. 108–117, Oct. 2001.

[13] J. A. Barsi, S. J. Hook, J. R. Schott, N. G. Raqueno, and B. L. Markham, "Landsat-5 thematic mapper thermal band calibration update," *IEEE Geosci. Remote Sens. Lett.*, vol. 4, no. 4, pp. 552–555, Oct. 2007.

[14] X. Hao, J. J. Qu, B. Hauss, and C. Wang, "A high-performance approach for brightness temperature inversion," *Int. J. Remote Sens.*, vol. 28, no. 21/22, pp. 4733–4743, 2007.

[15] G. Chander and B. Markham, "Revised Landsat-5 TM radiometric calibration procedures and postcalibration dynamic ranges," *IEEE Trans. Geosci. Remote Sens.*, vol. 41, no. 11, pp. 2674–2677, Nov. 2003.

[16] A. Beck, G. P. Anderson, P. K. Acharya, J. H. Chetwynd, L. S. Bernstein, E. P. Shettle, M. W. Matthew, and S. M. Adler-Golden, *MODTRAN4 User's Manual*. Hanscom AFB, MA: Air Force Res. Lab., 1999.

[17] F. Aires, A. Chédin, N. A. Scott, and W. B. Rossow, "A regularized neural net approach for retrieval of atmospheric and surface temperatures with the IASI instrument," *J. Appl. Meteorol.*, vol. 41, no. 2, pp. 144–159, Feb. 2002.

[18] A. Chédin, N. A. Scott, C. Wahiche, and P. Moulinier, "The improved initialization inversion method: A high resolution physical method for temperature retrievals from satellites of the TIROS-N series," *J. Clim. Appl. Meteorol.*, vol. 24, no. 2, pp. 128–143, Feb. 1985.

[19] V. Achard, "Trois Problèmes Clés de L'analyse Tridimensionelle de la Structure Thermodynamique de L'atmosphère par Satellite: Measure du Contenu en Ozone, Classification des Masses D'air, Modélisation Hyper-Rapide du Transfert Radiatif," Ph.D. dissertation, Université Pierre et Marie Curie, Paris, France, 1991.

[20] J. Escobar, "Base de Données Pour la Restitution de Paramètres Atmosphériques À L'échelle Globale; Étude Sur L'Inversion par Réseaux de Neurones des Données des Sondeurs Verticaux Atmosphériques Satellitaires Présents et à Venir," Ph.D. dissertation, Université Denis Diderot, Paris, France, 1993.

[21] F. Chevallier, F. Chéruy, N. A. Scott, and A. Chédin, "A neural network approach for a fast and accurate computation of a longwave radiative budget," *J. Appl. Meteorol.*, vol. 37, no. 11, pp. 1385–197, Nov. 1998.

[22] J. A. Sobrino, Z.-L. Li, and M. P. Stoll, "Impact of the atmospheric transmittance and total water vapor content in the algorithms for estimating satellite sea surface temperatures," *IEEE Trans. Geosci. Remote Sens.*, vol. 31, no. 5, pp. 946–952, Sep. 1993.

[23] C. François, A. Brisson, P. Le Borgne, and A. Marsouin, "Definition of a radiosounding database for sea surface brightness temperature simulations: Application to sea surface temperature retrieval algorithm determination," *Remote Sens. Environ.*, vol. 81, no. 2/3, pp. 309–326, Aug. 2002.

[24] J. C. Jiménez-Muñoz and J. A. Sobrino, "Feasibility of retrieving land-surface temperature from ASTER TIR bands using two-channel algorithms: A case study of agricultural areas," *IEEE Geosci. Remote Sens. Lett.*, vol. 4, no. 1, pp. 60–64, Jan. 2007.

[25] J. A. Sobrino, J. C. Jiménez-Muñoz, G. Sòria, M. Gómez, A. Barella-Ortiz, M. M. Zaragoza-Ivorra, Y. Julián, and J. Cuenca, "Thermal remote sensing in the framework of the SEN2FLEX project: Field measurements, airborne data and applications," *Int. J. Remote Sens.*, vol. 29, no. 17/18, pp. 4961–4991, 2008.
[26] T. N. Carlson and D. A. Ripley, "On the relation between NDVI, fractional vegetation cover, and leaf area index," *Remote Sens. Environ.*, vol. 62, no. 3, pp. 241–252, Dec. 1997.
[27] L. Guanter, M. C. González, and J. Moreno, "A method for the atmospheric correction of ENVISAT/MERIS data over land targets," *Int. J. Remote Sens.*, vol. 28, no. 3/4, pp. 709–728, 2007.
[28] D. A. Artis and W. H. Carnahan, "Survey of emissivity variability in thermography of urban areas," *Remote Sens. Environ.*, vol. 12, no. 4, pp. 313–329, Sep. 1982.

Juan C. Jiménez-Muñoz received the Ph.D. degree in physics from the University of Valencia, Valencia, Spain, in 2005.

He is currently a Research Scientist with the Global Change Unit, Department of Earth Physics and Thermodynamics, University of Valencia. His main research interests include thermal remote sensing and temperature/emissivity retrieval.

Jordi Cristóbal received the B.S. degree in biology, the M.S. degree in botany, and the M.S. degree in environmental sciences from the Autonomous University of Barcelona, Cerdanyola del Vallès, Spain, in 1996, 1998, and in 2003, respectively, and the M.S. degree in remote sensing and GIS from the Institute for Space Studies of Catalonia, Barcelona, Spain, in 1999. He is currently working toward the Ph.D. degree at the Autonomous University of Barcelona, focusing on forest evapotranspiration retrieval by means of medium and coarse spatial resolution remote sensing data and GIS modeling.

He is also currently an Associate Professor with the Department of Geography, Autonomous University of Barcelona. His main work has been done in climate modeling using remote sensing and geographical data, in thermal atmospheric corrections of satellite imagery, and in energy flux modeling. He has recently worked in water usage and snow coverage from long series of satellite images and in landscape modeling.

Prof. Cristóbal is a member of the GRUMETS (Research Group of Methods in Remote Sensing and GIS).

José A. Sobrino received the Ph.D. degree in physics from the University Of Valencia, Valencia, Spain in 1989.

He is currently a Professor of physics and remote sensing and the Head of the Global Change Unit (http://www.uv.es/ucg), Department of Earth Physics and Thermodynamics, University of Valencia, Valencia, Spain. He is the author of more than 100 papers and a Coordinator of the European projects WATERMED and EAGLE. His research interest include atmospheric correction in visible and infrared domains, the retrieval of emissivity and surface temperature from satellite images, and the development of remote sensing methods for land cover dynamic monitoring.

Prof. Sobrino has been a member of the Earth Science Advisory Committee of the European Space Agency since November 2003. He is the Chairperson of First and Second International Symposium RAQRS (Recent Advances in Quantitative Remote Sensing) http://www.uv.es/raqrs.

Guillem Sòria received the Ph.D. degree in physics from the University of Valencia, Valencia, Spain, in 2006.

He is currently a Research Scientist with the Global Change Unit, Department of Earth Physics and Thermodynamics, University of Valencia. His present investigation includes the retrieval of surface temperature, including land, ice, and sea through multichannel and multiangle algorithms from thermal-infrared remotely sensed data supplied by ATSR-1, ATSR-2, and ENVISAT-AATSR sensors.

Miquel Ninyerola received the B.S. degree in biology and the Ph.D. degree in GIS modeling from the Autonomous University of Barcelona, Cerdanyola del Vallès, Spain, in 1994 and 2001, respectively.

First, his research focused on climatological mapping by combining spatial interpolation, multivariate statistics, and GIS. In addition, he developed DEM-based solar radiation maps and climatic-envelope-based vegetation suitability maps. He has recently worked on refining (mainly by introducing remote sensing information) and applying these climatic and suitability models in fields such as landscape ecology, natural hazards, or plant ecophysiology. He is currently a Full Professor with the Department of Animal Biology, Plant Biology and Ecology, Autonomous University of Barcelona. His current research deals with statistical downscaling techniques to develop future climatic scenarios where to project the present-day vegetation suitability models.

Prof. Ninyerola is a member of the GRUMETS (Research Group of Methods in Remote Sensing and GIS).

Xavier Pons received the B.S. degree in biology, the M.S. degree in botany, and the Ph.D. degree in remote sensing and GIS from the Autonomous University of Barcelona, Cerdanyola del Vallès, Spain, in 1988, 1990, and, 1992, respectively.

His main work has been done in radiometric and geometric corrections of satellite imagery, in cartography of ecological and forest parameters from airborne sensors, in studies of the spectral response of Mediterranean vegetation, and in GIS development, both in terms of data structure and organization and in terms of software writing (MiraMon). He has recently worked in descriptive climatology models, in modeling forest fire hazards, and in analysis of landscape changes, water usage, and snow coverage from long series of satellite images. He is currently working in the implications of image compression on remote sensing. He is currently a Full Professor with the Department of Geography, Autonomous University of Barcelona, and coordinates research activities in GIS and remote sensing with the Centre for Ecological Research and Forestry Applications, Cerdanyola del Vallès.

Prof. Pons is a member of the GRUMETS (Research Group of Methods in Remote Sensing and GIS).